Earth and Planetary Science Letters 582 (2022) 117419

Contents lists available at ScienceDirect

Earth and Planetary Science Letters

www.elsevier.com/locate/epsl

Sulfate-limited euxinic seawater facilitated Paleozoic massively bedded barite deposition

Tao Han [a], Yongbo Peng [b,c], Huiming Bao [b,c,*]

[a] State Key Laboratory of Ore Deposit Geochemistry, Institute of Geochemistry, Chinese Academy of Sciences, Guiyang 550081, China
[b] International Center for Isotope Effects Research, Nanjing University, Nanjing, 210023, China
[c] School of Earth Sciences and Engineering, Nanjing University, Nanjing, 210023, China

ARTICLE INFO

Article history:
Received 24 August 2021
Received in revised form 15 January 2022
Accepted 6 February 2022
Available online 22 February 2022
Editor: B. Wing

Keywords:
seawater sulfate
oceanic redox structure
Ba^{2+} accumulation
barite, zinc sulfides
hyalophane, hydrothermal

ABSTRACT

Existing models for massively bedded barite (MBB) deposits (e.g., sedimentary exhalative and diagenetic/cold-seep) satisfy some geological and geochemical observations, but none explain the Paleozoic clustering of MBB deposits in Earth history. Here we bring seawater redox history into the picture and propose a sulfate-limited euxinic seawater (SLES) model where hydrothermally sourced Ba^{2+} accumulates as dissolved ion while other metal ions precipitate as insoluble metal sulfides. A subsequent encounter of this Ba^{2+}-rich water mass with a sulfate-bearing one results in the deposition of MBB, thus physically separated from the accompanied metal sulfide deposits. We tested the SLES model using early Cambrian MBB deposits in South China through petrographic and isotope analyses. Syngenetic sphalerite and barite layers show a clear separation. A wide range of $^{87}Sr/^{86}Sr$ values (0.7082 to 0.7120) of the MBB supports a mixing of seawater and hydrothermal sources. A large range of $\delta^{34}S$ values (32.2 to 61.1‰) of the MBB and the occurrence of mineral hyalophane supports an overall sulfate-limited but sulfate-concentration temporally and spatially heterogeneous ocean. Our model established the genetic link between MBB deposits and the accompanied metal sulfide deposits in the Paleozoic. The dearth of MBB deposits before and after the Paleozoic is due to widespread ferruginous oceans with little sulfate and complete oxygenated oceans with too much sulfate, respectively. The Paleozoic clustering of the MBB deposits is a consequence of a critical redox transition in Earth history.

1. Introduction

Barite is a common mineral which occurs in a variety of geological environments, for example, as disseminated minerals in clastic and chemical sediments, cold-seeps, and as an associated mineral in volcanogenic massive sulfide or Mississippi Valley-type Zn–Pb sulfide deposits (Hanor, 2000). However, we and others included (Jewell, 2000; Torres et al., 2003) have noticed that massively bedded barite (MBB) deposits, usually in high grades (up to 90 wt.%) and in tens of million tonnes, cluster temporally in the Paleozoic (i.e., from Cambrian to Carboniferous; Fig. 1; Supplementary Table 1). These MBB deposits are often a few to tens of meters in thickness and hosted in siliciclastic, carbonaceous rocks without significant amounts of associated volcanic materials (Jewell, 2000; Clark et al., 2004). Importantly, MBB deposits are sometimes accompanied by clastic-dominant (or CD-type) Zn–Pb sulfide deposits of greater commercial value, e.g., late Devonian Zn–Pb–Ba deposits in Selwyn Basin and late Mississippian Zn–Pb–Ba deposits in Red Dog, Alaska (Goodfellow, 1987; Maynard and Okita, 1991; Johnson et al., 2004; Magnall et al., 2016). However, some MBB deposits have no known co-occurring metal sulfide deposits of commercial value, e.g., the early Cambrian MBB deposits in South China and the late Devonian MBB deposits in Nevada, U.S.A. (Jewell and Stallard, 1991; Wang and Li, 1991). A sound MBB formation model could offer guidance on CD-type Zn–Pb sulfide ore prospecting.

In an attempt to explain the association and non-association of the metal sulfide and MBB deposits, researchers proposed a scenario in which sedimentary exhalative (SedEx) brines were introduced into euxinic seawater (Goodfellow, 1987). The model requires two unrelated, discrete types of brines, oxidized ("SO_4^{2-}-predominant") one evolved from carbonates/evaporites basins and reduced ("H_2S-predominant") one from siliciclastic shale basins, respectively (Cooke et al., 2000; Table 1). This two-brine SedEx model was used to explain the lack of an MBB deposit in the Proterozoic Zn–Pb deposit in McArthur Basin (i.e., oxidized brines) and the presence of an accompanied MBB deposit in the Paleozoic

* Corresponding author at: International Center for Isotope Effects Research, Nanjing University, Nanjing, 210023, China.
E-mail address: bao@nju.edu.cn (H. Bao).

https://doi.org/10.1016/j.epsl.2022.117419
0012-821X/

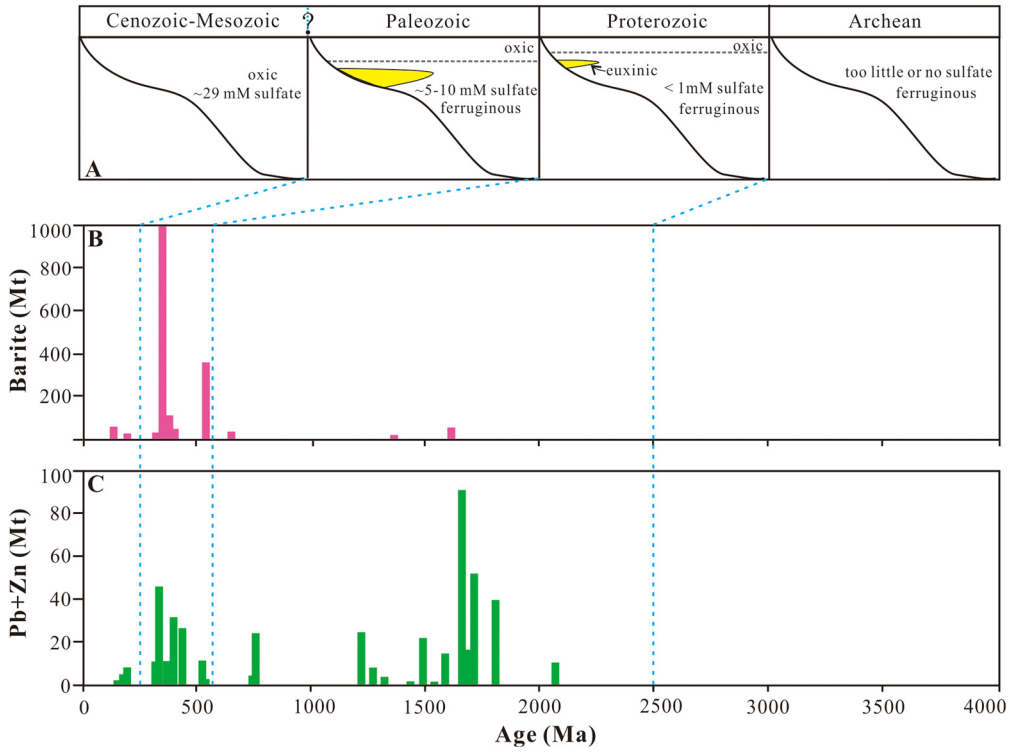

Fig. 1. Distribution of sedimentary ore deposits in Earth history. A: secular variation of seawater sulfate concentration (Algeo et al., 2015; Fakhraee et al., 2019) and the changing ocean redox structure along continental shelf (Canfield, 2005; Lyons et al., 2014; Li et al., 2010; Poulton and Canfield, 2011; Sperling et al., 2021); the "?" marks some uncertainty in time when the ocean redox state changed from dynamically stratified to fully oxygenated; B: MBB deposits (data from Supplementary Table 1); C: CD-type Zn–Pb sulfide deposits (Leach et al., 2010); "Mt" stands for "million tonnes". The width of the vertical bars is uniform for all occurrences.

Table 1
Proposed formation models for massively bedded barite (MBB) deposits.

Model	Sedimentary exhalative (SEDEX) model	Diagenetic/cold-seep model	Sulfate-limited euxinic seawater (SLES) model
Description	Oxidized bines (SO_4^{2-}-predominant) and reduced, acidic brines (H_2S-predominant) are introduced into euxinic seawater, resulting in Pb-Zn deposits and Pb-Zn-MBB deposits, respectively	Ba^{2+}-rich fluids are derived from organic-rich and highly reducing sediments, and MBB deposits form at cold seeps or in sediments during early diagenesis	The same metal-rich brine encounters sulfate-limited euxinic water during which metal sulfides precipitate but dissolved Ba^{2+} accumulates. The accumulated Ba^{2+} precipitates as MBB deposits upon encountering sulfate-bearing water in different space or time
S source	Sulfate in seawater	Sulfate in seawater or porewater	Sulfate in seawater
Ba source	Hydrothermal fluids	Sedimentary organic matter	Hydrothermal fluids
Secular pattern	Not specified	Not specified	Temporally clustered in the Paleozoic
References	Cooke et al., 2000	Jewell and Stallard, 1991; Torres et al., 2003; Johnson et al., 2009; Canet et al., 2014; Magnall et al., 2016; Xu et al., 2016; Fernandes et al., 2017	this study

Zn–Pb deposit in Selwyn Basin (i.e., reduced brines). However, the redox state of a brine should depend on the evolving geochemistry (e.g., sulfate reduction) of the brine, not necessarily the redox state of the lithology in a basin. For example, the vent fluids/brines in modern seafloor hydrothermal fields are often rich in H_2S with little sulfate despite the fact that the brines were initially seawater rich in sulfate (Humphris and Klein, 2018 and references therein).

Later on, a number of studies suggest that the MBB deposits formed early diagenetically or in settings like cold seeps in sea floor (i.e., diagenetic/cold-seep model) (Table 1; Jewell and Stallard, 1991; Torres et al., 2003; Johnson et al., 2009; Canet et al., 2014; Magnall et al., 2016; Xu et al., 2016; Fernandes et al., 2017). The diagenetic/cold-seep model has the sulfate derived from porewater/seawater and barium from local sediments including the organic matter within. A major problem with this diagenetic/cold-seep model is the observed large quantity of Ba and high-purity of $BaSO_4$ in the laterally extensive MBB deposits. Importantly, both the two-brine SedEx and diagenetic/cold-seep models have failed to explain the temporally clustered occurrence of MBB deposits in the Paleozoic (Fig. 1).

Sulfate-limited euxinic seawater (SLES) model

Here, we propose a sulfate-limited euxinic seawater (SLES) model for the MBB deposits (listed in Table 1). Hydrothermally sourced metal ions (e.g., Ba^{2+}, Zn^{2+} and Pb^{2+}) meet with locally sulfate (SO_4^{2-})-limited, hydrogen sulfide (H_2S)-rich water column (i.e., euxinic). When that happens, Zn^{2+} and Pb^{2+} ions precipitate

out of the water mass as insoluble sulfide solids whereas Ba^{2+} remains largely as a soluble ion until it encounters a SO_4^{2-}-rich water and precipitates as $BaSO_4$. The crux of SLES model is in the metal ion behaviors: 1) Ba^{2+} does not form an insoluble solid whereas the base metal ions do when encountering H_2S-bearing, SO_4^{2-}-free water; 2) Only Ba^{2+} forms a solid whereas the base metal ions do not when encountering SO_4^{2-}-bearing, H_2S-free water; 3) Ba^{2+} precipitates as barite crystals and base metal ions precipitate as sulfide solids when encountering a euxinic water mass bearing both SO_4^{2-} and H_2S; 4) Barite crystals are susceptible to dissolution if an organic-rich, sulfate-limited anoxic water mass returns (Bolze et al., 1974; Ouyang et al., 2018); and 5) Ba^{2+} may precipitate as witherite when encountering SO_4^{2-}-limited, CO_3^{2-}-rich water. Considering an overall intermediate seawater sulfate concentration (Algeo et al., 2015; Li et al., 2010; Fakhraee et al., 2019) and a transitional oxygenation state in Earth history (Canfield, 2005; Li et al., 2010; Sperling et al., 2021), the Paleozoic oceans would have had oxic, euxinic, and ferruginous water masses co-existed spatial-temporally, a condition facilitated the deposition of most MBB deposits in Earth history as well as some high-grade base metal sulfide deposits (Fig. 1B-C).

The SLES model predicts that 1) there should be cases where MBB and sulfide deposits are genetically related but physically separated due to the spatial-temporal heterogeneity of the sulfate and H_2S concentrations in Paleozoic oceans; 2) there should be a wide range of strontium isotope composition ($^{87}Sr/^{86}Sr$) in the MBB deposits because of the different mixing ratios between sulfate-rich seawater and metal-rich hydrothermal brines; 3) there should be a large range of sulfur isotope composition ($\delta^{34}S$) in the MBB deposits because of the $\delta^{34}S$ sensitivity to degrees of microbial sulfate reduction (MSR) in a SO_4^{2-}-limited euxinic water mass. These predictions have been confirmed in a few Paleozoic MBB deposits, but not in others, especially in those historically regarded as barite-only ore deposits, e.g., the lower Cambrian MBB deposits in South China. If the SLES model is sound, the South China MBB deposits should have the same features. In particular, we should find an accompanied, physically separated occurrence of sulfide deposits or characteristic minerals, e.g., those deposited in Ba-rich and sulfate-free mixed water. To test these predictions, we examined the lower Cambrian MBB deposits and potential sulfide deposits in South China and compiled published data of well-studied MBB deposits worldwide for comparison (Supplementary materials). Petrographic observation was conducted including texture relationship between barite and sulfides. We also adopted a sodium carbonate technique for Sr isotope (Breit et al., 1985) and a chelating method (Bao, 2006) for S isotope pretreatment, in measuring the lower Cambrian MBB samples in South China.

2. Materials and methods

2.1. Geological background and the lower Cambrian MBB samples, South China

The South China Block consists of the Yangtze platform, Nanhua basin, and Cathaysian platform which was assembled during the Neoproterozoic (Fig. 2A; Feng et al., 2002; Li et al., 2008). The well-preserved sedimentary strata are generally dominated by carbonates at shallow-water and black shale/chert at slope and basin settings during the early Cambrian (Chen et al., 2009). Lower Cambrian MBB deposits in South China are hosted near the top of the Liuchapo Formation in Nanhua Basin where basinal facies were deposited with a radiometric age of ~522–524 Ma (Chen et al., 2015). In particular, the MBB ores occur beneath massive chert layers, chert and thin black shale layers, phosphorus nodules, and limestone concretions in an ascending order, and are overlain by interbedded chert and black shales again. The Liuchapo Formation itself is overlain conformably by the lower Cambrian Niutitang massive black shale and underlain by the Ediacaran Doushantuo dolostone (Fig. 2B). Samples of the lower Cambrian MBB deposits and nearby chert/shale samples were collected from the open pits and outcrops at Tianzhu (27°00′N, 109°06′E) and Zhengyuan (27°08′N, 108°52′E), two counties in Guizhou Province in southern China (Fig. 2). Massive, banded, or disseminated barite ores and barite nodules of a few to ten meters in thickness occur commonly in the Liuchapo Formation chert. While surveying MBB deposits worldwide and throughout the Proterozoic and Phanerozoic, we compiled those that are published and have age information and are indeed hosted chert and black shales.

2.2. Petrographic-isotope methods

Texture relationship between barite and potential metal sulfides in the lower Cambrian in South China was examined using FEI Scios DualBeam field emission scanning electron microscope (FE-SEM) equipped with EDAX Energy Dispersive Spectroscopy (EDS) at Institute of Geochemistry, Chinese Academy of Sciences (IGCAS). Backscattered electron (BSE) mode and point analyses of EDS were used to identify the minerals and texture relationship.

Barite samples were powdered and pretreated using hydrofluoric acid and nitric acid solutions to remove quartz, carbonate, and sulfide minerals and then dissolved using aqueous sodium carbonate, followed by Sr separation through ion exchange (Breit et al., 1985). The $^{87}Sr/^{86}Sr$ was measured on a Nu Plasma III multiple-collector inductively coupled plasma mass spectrometer (MC-ICP-MS) at IGCAS. NIST SRM987 with an average $^{87}Sr/^{86}Sr$ value of 0.710248 ± 0.000004 (2SD, n=10) was used as the reference to monitor and correct drifts of the instrument. For $\delta^{34}S$, barite samples were first treated using a diethylenetriaminepentaacetic-acid dissolution and re-precipitation (DDARP) method (Bao, 2006) and then measured in continuous-flow mode using a Vario Microcube connected to an Isoprime 100 at Department of Geology & Geophysics, Louisiana State University. The $\delta^{34}S$ values were reported relative to the Vienna-Canyon Diablo Troilite (V-CDT) with a standard deviation at $\pm 0.3‰$ on basis of long-term analyses of in-house standards and samples. Both $\delta^{34}S$ and Sr isotope ratio were measured once for each drilled sample powder in this study.

3. Results

A compilation of published MBB deposits worldwide displays a clear clustering in the Paleozoic (Fig. 1B). High purity (up to 90%) and lack of clastic minerals (e.g., clays) are characteristic of the MBB ores (Fig. 3A–B) in South China. Quartz is the main matrix mineral (Fig. 3B). Finely laminated sphalerite layers consist of ZnS grains and they coexist with grains of hyalophane ($(K,Ba)[Al(Si,Al)Si_2O_8]$), a Ba-silicate mineral (Fig. 3C-D). The $^{87}Sr/^{86}Sr$ values range from 0.7082 to 0.7120 (Fig. 4A; Supplementary Table 2) and the $\delta^{34}S$ values range from 32.2 to 61.1‰ (Fig. 4B; Supplementary Table 3) for the lower Cambrian MBB samples. Newly obtained isotope data from lower Cambrian South China are gathered with those of published MBB deposits (Fig. 4 and Supplementary Tables 2–3).

4. Discussion

4.1. Co-occurring MBB and metal sulfide deposits

A key difference between the SLES and the diagenetic/cold-seep models for MBB deposits is that the former advocates a genetic

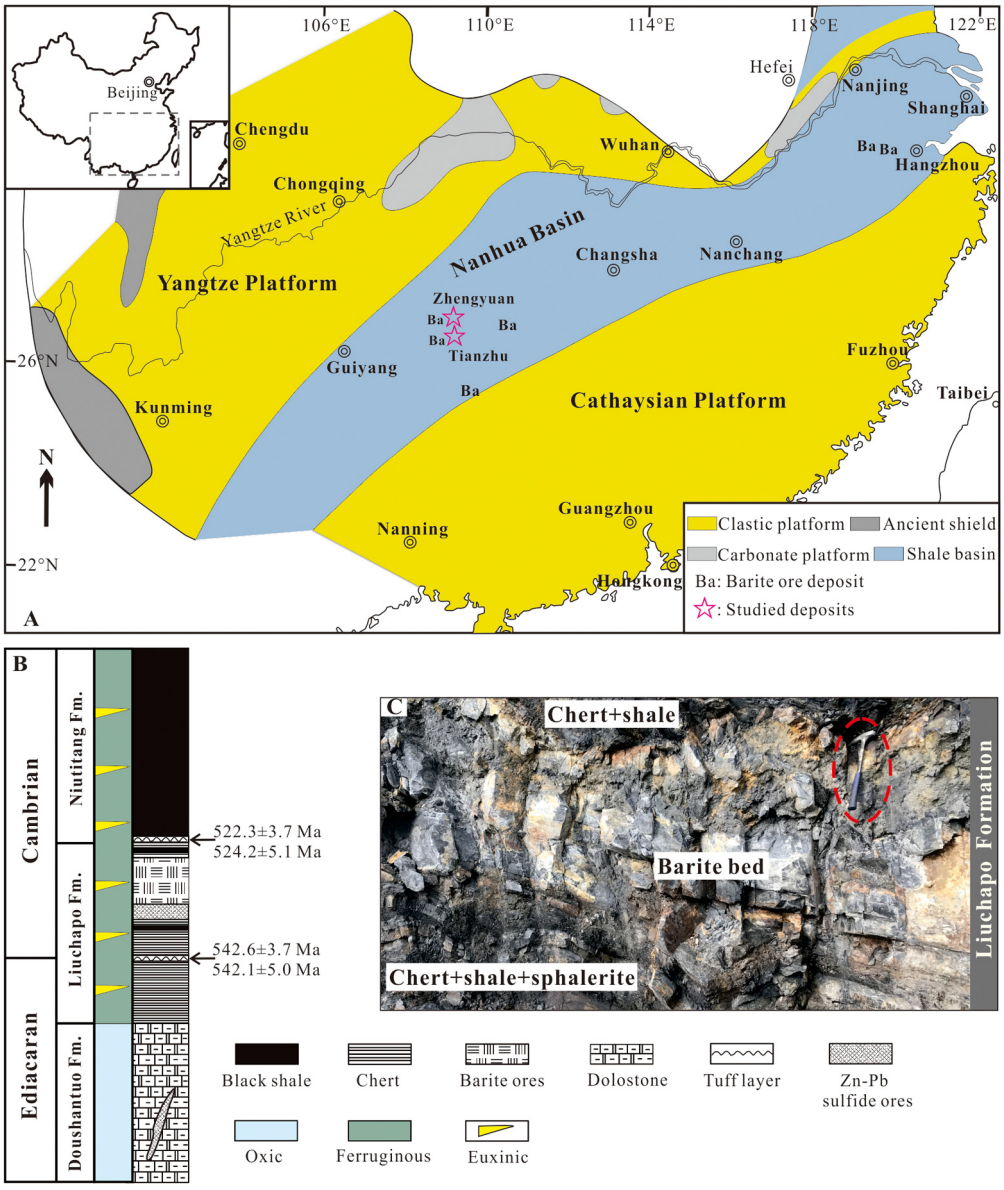

Fig. 2. Geological background of the lower Cambrian massively bedded barite deposits in South China. A: lithofacies paleogeography of South China during the Early Cambrian and the studied locations (modified from Feng et al., 2002; Li et al., 2008); B, a composite stratigraphic section across Ediacaran to Cambrian in Guizhou Province, South China; and radioactive ages from references (Chen et al., 2015) and the ferruginous conditions with euxinic wedges at the slope/basin settings across the Ediacaran-Cambrian transition, South China from Wang et al. (2012) and Jin et al. (2016); (C), an outcrop of a massively bedded barite ores hosted in an interbedded chert and black shale sequence in Tianzhu County, Guizhou Province.

link between the MBB and sulfide deposits whereas the latter does not (Table 1). Our petrologic observation shows that not only sphalerite (ZnS) co-occurs with bedded barites but also the barite and sphalerite layers are separated into two high-purity mineral phases (Fig. 3A–B). This physical separation and the high-purity nature of the sphalerite and the barite layers (Fig. 3A–B) suggests that Zn^{2+} precipitates as ZnS when a metal-rich water mass or brine encounters H_2S-rich water while in the meantime dissolved Ba^{2+} is able to accumulate in sulfate-free water and later precipitated as a barite layer after encountering SO_4^{2-}-bearing water. These separate yet high-purity mineral phases suggest that they were precipitated in water column and not in sediment, thus are consistent with the SLES model. In addition, the SLES predicts a scenario in which excess Ba^{2+} will be available after exhausting all sulfate in initially sulfate-limited water. The existence of such a condition is confirmed by the occurrence of hyalophane, a barium silicate, not a barium sulfate mineral, in the adjacent black shales (Fig. 3C–D).

Although our newly discovered sulfide deposits are inconspicuously thin sulfide layers, it overturns the decades-old view that the lower Cambrian MBB deposit in South China is a barite-only ore deposit. We recognize that in some MBB deposits in the world no metal sulfide deposits of economic value have been found in the vicinity despite much effort. One possibility is that the local hydrothermal fluids were poor in metals or the basins had a high flux of detrital materials, which diluted the metal content.

4.2. Wide ranges of Sr and S isotope compositions in an MBB deposit

The SLES model prediction is confirmed by the wide range $^{87}Sr/^{86}Sr$ values. Sr isotope ratio of the MBB deposits has been measured extensively for metal source tracing (Fig. 4A; Supplementary Table 2). The lower Cambrian MBB samples have a wide range of $^{87}Sr/^{86}Sr$ values (0.7082 to 0.7120) which are higher, thus, more radiogenic than that of the early Cambrian seawater (~0.7082) (Li et al., 2013). Other Paleozoic MBB deposits also have

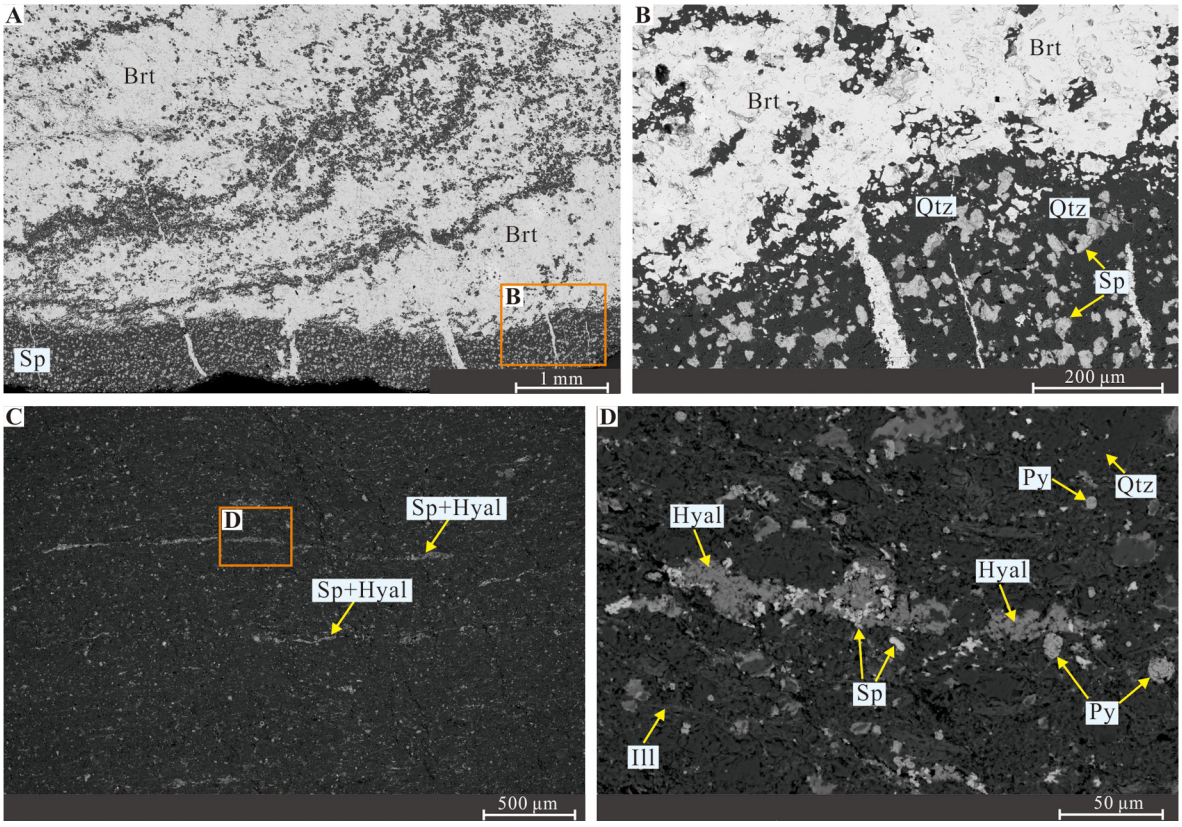

Fig. 3. Texture relationship between bedded barite and sulfide layers in the lower Cambrian Liuchapo Formation, Tianzhu, Guizhou Province, China. A: alternating sphalerite and barite layers; B: an enlarged image with barite cutting through sphalerite in A; C: a sulfide-rich shale sample in the vicinity of a barite bed; D: an enlarged image showing coexisting sphalerite and hyalophane in C. Abbreviations: Qtz: quartz; Brt: barite; Sp: sphalerite; Hyal: hyalophane; Py: pyrite; Ill: illite.

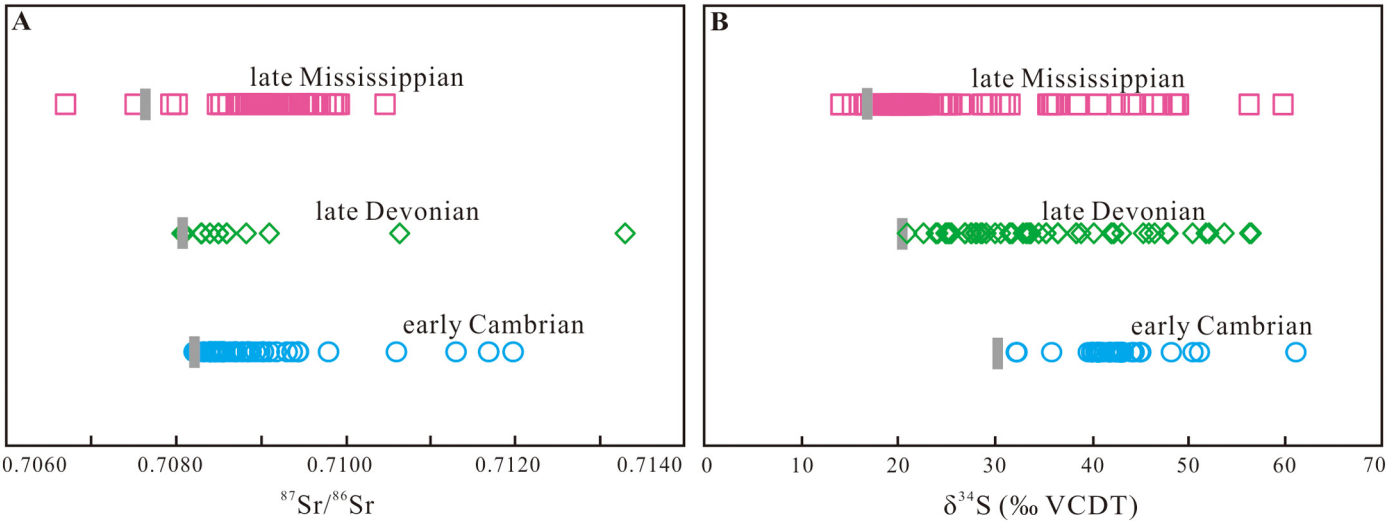

Fig. 4. A compilation of $^{87}Sr/^{86}Sr$ (A) and $\delta^{34}S$ (B) values of Paleozoic MBB deposits. Grey bars are the respective $^{87}Sr/^{86}Sr$ and $\delta^{34}S$ values of the coeval seawater. The data from late Devonian MBB deposits in Nevada and Selwyn, and late Mississippian ones in Red Dog of Alaska were compiled together with those from the early Cambrian MBB deposits in South China. All data can be found in Supplementary Table 2–3.

higher $^{87}Sr/^{86}Sr$ values than their coeval seawaters (Fig. 4A). Although there is no direct evidence for hydrothermal fluid chemistry, recent studies inferred that metal cations for CD-type Zn–Pb deposits may be extracted from basement rocks of multiple sources, including sedimentary rocks and/or felsic rocks (Ayuso et al., 2004; Gigon et al., 2020). Hydrothermal fluid can often have low $^{87}Sr/^{86}Sr$ values (e.g., 0.704–0.707) (Paytan et al., 2002) or inherit high $^{87}Sr/^{86}Sr$ values (e.g., up to 0.720) through interacting with clastic materials (Emsbo and Johnson, 2004).

The large $\delta^{34}S$ range (32.2 to 61.1‰; Fig. 4B; Supplementary Table 3) of the South China MBB deposits is also consistent with the SLES model prediction. All the $\delta^{34}S$ values are higher than that of the coeval early Cambrian seawater (~30‰; Kampschulte and Strauss, 2004), a pattern also observed in other Paleozoic MBB deposits in the world (Fig. 4B), supporting a sulfate-limited seawater (Canfield et al., 2010). When sulfate is limited, MSR can drive the remaining sulfate extremely high in its $\delta^{34}S$ value. Once sulfate is consumed to a sufficiently low concentration, a small amount

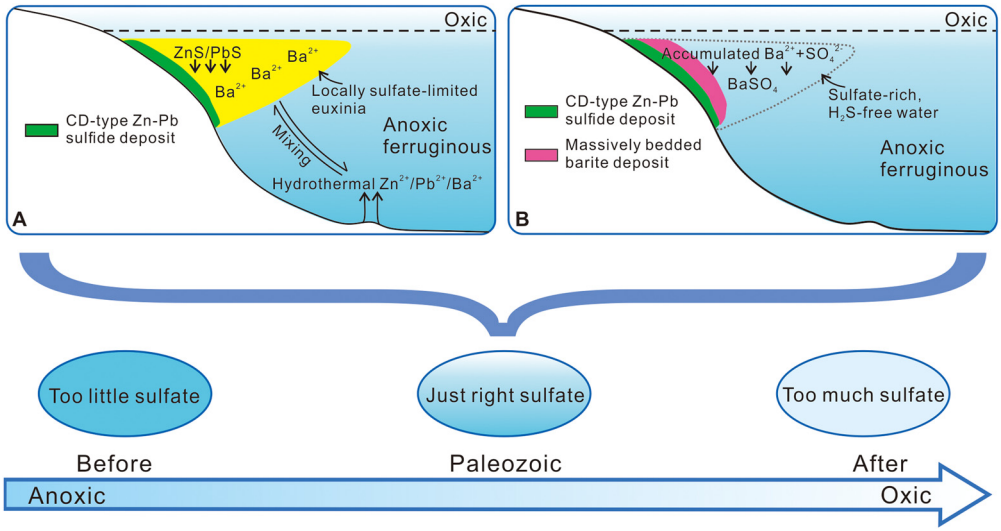

Fig. 5. Cartoons illustrating the sulfate-limited euxinic seawater (SLES) model and seawater sulfate concentration history. Dynamic coexistence of oxic, euxinic (sulfate-limited), and ferruginous water masses was prevalent in the Paleozoic ocean, which favored the deposition of MBB and associated CD-type sulfide deposits. A: hydrothermal sourced Zn^{2+}, Pb^{2+} and Ba^{2+} cations encounter locally sulfate-limited euxinic water, resulting in the CD-type Zn–Pb sulfide deposits and the accumulation of excess dissolved Ba^{2+}; B: MBB precipitation occurs when the accumulated Ba^{2+} in SO_4^{2-}-free euxinic water encounters new SO_4^{2-}-rich water.

of Ba^{2+} can precipitate out the remaining sulfate, usually with high $\delta^{34}S$ values. If the process continues, the water body would become SO_4^{2-}-free, which allows Ba^{2+} to accumulate. The accumulated Ba^{2+} would then precipitate to form a high-purity MBB deposit when encountering new SO_4^{2-}-bearing water. Although large $\delta^{34}S$ range and high $\delta^{34}S$ values can also be generated in sedimentary pore water during diagenesis, the high purity of barite and the near-absence of clastic materials (e.g., clay, Fig. 3) support a water-column barite precipitation.

4.3. Paleozoic clustering of MBB deposits

Our compilation of the MBB deposits worldwide reveals a Paleozoic cluster (Fig. 1B), a phenomenon also recognized by previous review (Jewell, 2000; Torres et al., 2003). As shown, the SLES model explains most sedimentological, petrographic, and geochemical observations of the Paleozoic MBB deposits (Fig. 5). The model also explains the Paleozoic clustering of MBB deposits. It is recognized that the ocean evolved from anoxic, ferruginous state in the Archean to dynamically redox-stratified one with transient euxinic wedges along some shorelines during much of the Proterozoic Eon to Paleozoic Era, and gradually changed into an oxygenated ocean during the Mesozoic and Cenozoic (Canfield, 2005; Li et al., 2010; Poulton and Canfield, 2011; Lyons et al., 2014; Sperling et al., 2021). This secular trend of ocean redox conditions should have dictated much of the sedimentary and geochemical processes including sulfate abundance and, therefore, the temporal window favorable for MBB or metal sulfide deposits. The seawater sulfate content is believed to be low (<1 mM) during the Archean and much of the Proterozoic Eon (Fakhraee et al., 2019) but was likely as high as that of present-day (~29 mM) during the Mesozoic and Cenozoic (Algeo et al., 2015). It is difficult for either MBB or CD-type Zn–Pb deposits to precipitate when there was little sulfate in the oceans. When seawater was fully oxygenated in the Mesozoic and Cenozoic, most organic matter is oxidized by dissolved O_2 and very little MSR is occurring in water column, resulting in the dearth of sulfate-limited euxinic water and the lack of MBB or associated sulfide deposits.

When the seawater sulfate was at an intermediate level, say at ~5 to 10 mM during the Paleozoic (Algeo et al., 2015), it becomes conducive for spatially and temporally heterogeneous ocean redox conditions in which locally either Ba^{2+} accumulates when sulfate is extremely low (i.e., all in H_2S and HS^-) or metal ions (Pb^{2+} and Zn^{2+}) accumulate when H_2S and HS^- is extremely low (i.e., all in sulfate) in euxinic water mass. The fluctuating H_2S-rich and SO_4^{2-}-rich water in space and time leads to the MBB and CD-type Zn–Pb deposits during the Paleozoic era. There are Proterozoic cases where only CD-type Zn–Pb deposits were formed (Fig. 1C; Leach et al., 2010). The lack of accompanied MBB deposits in the Proterozoic Eon may be explained by the exhaustion of sulfate in the much low-sulfate oceans (<1 mM; Fakhraee et al., 2019) after Zn–Pb sulfide precipitation (Fig. 1), being consistent with the overall much more reduced surface Earth than the Paleozoic.

A quantitative estimate of this "intermediate" seawater sulfate concentration in the Paleozoic would be informative. In this study, when we refer to "sulfate-limited", we mean an overall lower concentration in the Paleozoic than the Present to the extent that the oxic, euxinic, and ferruginous water masses often co-existed spatial-temporally and when encountering a water mass containing hydrothermally accumulated Ba^{2+}, all sulfate could sometimes be precipitated as $BaSO_4$. The exact sulfate concentration in a water mass is a moving target. However, since we have encountered many cases where after the deposition of barite beds and there were still excess Ba^{2+} left to form mineral hyalophane, if we could somehow place an upper-limit constraint on the Ba^{2+} concentration in a hydrothermally fed bottom water mass, that Ba^{2+} concentration may be regarded as the typical upper-limit for seawater sulfate concentration of the Paleozoic. Such a Ba^{2+} constraint, if obtainable, may add an independent proxy for past seawater sulfate concentration in addition to the rate method, i.e., modeling using the maximum observed rate of seawater sulfate $\delta^{34}S$ change and the $\delta^{34}S$ difference between cogenetic sedimentary sulfate and sulfide, and the empirical MSR-trend method (Algeo et al., 2015).

The Paleozoic clustering of MBB deposits is a consequence of a critical redox transition in Earth history. The MBB deposits require a right fluctuation of sulfate concentration in euxinic seawater. Sulfate-limited euxinic water allowed SO_4^{2-}-free and SO_4^{2-}-rich water bodies to be dynamically available in space and time and thus Ba^{2+} accumulated in SO_4^{2-}-free water and barite precipitated in massive quantities when the water encountering a SO_4^{2-}-rich water, a condition prevalent in Paleozoic oceans.

The Paleoarchean barite deposits in South Africa and in Western Australia are special in themselves, not only in their origin as evident from their unique S-MIF signatures (Bao et al., 2007) but

also in the total absence of sedimentary barite beds in the next, at least 1 billion yr in Earth history (Jewell, 2000). Our SLES model does not apply to the Paleoarchean barite deposits.

5. Conclusions

The SLES model builds upon previous SedEx and diagenetic/cold-seep models and yet is more accommodating to the observed geological, petrographic, elemental, and isotope data.

1) The SLES model supports a genetic relationship between MBB and metal sulfide deposits in that Ba^{2+} and other base metal ions (Zn^{2+}, Pb^{2+}) have a significant hydrothermal contribution. In the vicinity of an MBB deposit, there is a high probability of base metal sulfide deposits.

2) The SLES model brings secular history of seawater redox evolution and sulfate concentration into understanding the origin of the MBB and associated metal sulfide deposits in geological record. The MBB deposits occurred mostly in a backdrop of moderate Paleozoic seawater sulfate concentrations which were conducive to the co-existence of oxic, euxinic, and ferruginous water masses in shallow oceans. Before and after the Paleozoic Era, the atmosphere-hydrosphere was too reduced and too oxidized, respectively, to have significant sizes of euxinic water mass for MBB deposition.

CRediT authorship contribution statement

Tao Han: conceptualization, data acquisition, writing – original draft. **Yongbo Peng:** Data acquisition, review. **Huiming Bao:** conceptualization, investigation, writing and editing.

Declaration of competing interest

The authors declare that they have no known competing financial interests or personal relationships that could have appeared to influence the work reported in this paper.

Acknowledgements

This work benefited from discussion with colleagues who advocate SedEx and diagenetic/cold-seep models. Many thanks to Hao Yan, Pengfei Zuo, Haoran Ma, Youwei Chen, Youqiang Qi and Zhitong Lu for their assistance with laboratory analyses and discussion. Financial support was provided by the National Natural Science Foundation of China (U1812402, 41890841, 41873056, 42173001), the Strategic Priority Research Program (B) of Chinese Academy of Sciences (CAS) (XDB18030302, XDB18010104), and CAS "Light of West China" Program.

Appendix A. Supplementary material

Supplementary material related to this article can be found online at https://doi.org/10.1016/j.epsl.2022.117419.

References

Algeo, T.J., Luo, G.M., Song, H.Y., Lyons, T.W., Canfield, D.E., 2015. Reconstruction of secular variation in seawater sulfate concentrations. Biogeosciences 12, 2131–2151. https://doi.org/10.5194/bg-12-2131-2015.

Ayuso, R.A., Kelley, K.D., Leach, D.L., Young, L.E., 2004. Origin of the Red Dog Zn–Pb-Ag deposits, Brooks Range, Alaska: evidence from regional Pb and Sr isotope sources. Econ. Geol. 99, 1533–1553. https://doi.org/10.2113/gsecongeo.99.7.1533.

Bao, H., 2006. Purifying barite for oxygen isotope measurement by dissolution and reprecipitation in a chelating solution. Anal. Chem. 78, 304–309. https://doi.org/10.1021/ac051568z.

Bao, H., Rumble III, D., Lowe, D.R., 2007. The five stable isotope compositions of Fig Tree barites: implications on sulfur cycle in ca. 3.2 Ga oceans. Geochim. Cosmochim. Acta 71, 4868–4879. https://doi.org/10.1016/j.gca.2007.05.032.

Bolze, C.E., Malone, P.G., Smith, M.J., 1974. Microbial mobilization of barite. Chem. Geol. 13, 141–143. https://doi.org/10.1016/0009-2541(74)90006-0.

Breit, G.N., Simmons, E.C., Goldhaber, M.B., 1985. Dissolution of barite for the analysis of strontium isotopes and other chemical and isotopic variations using aqueous sodium carbonate. Chem. Geol. 52, 333–336. https://doi.org/10.1016/0168-9622(85)90043-0.

Canet, C., Anadón, P., González-Partida, E., Alfonso, P., Rajabi, A., Pérez-Segura, E., Alba-Aldave, L.A., 2014. Paleozoic bedded barite deposits from Sonora (NW Mexico): evidence for a hydrocarbon seep environment of formation. Ore Geol. Rev. 56, 292–300. https://doi.org/10.1016/j.oregeorev.2013.06.009.

Canfield, D.E., 2005. The early history of atmospheric oxygen: homage to Robert M. Garrels. Annu. Rev. Earth Planet. Sci. 33, 1–36. https://doi.org/10.1146/annurev.earth.33.092203.122711.

Canfield, D.E., Farquhar, J., Zerkle, A.L., 2010. High isotope fractionations during sulfate reduction in a low-sulfate euxinic ocean analog. Geology 38, 415–418. https://doi.org/10.1130/G30723.1.

Chen, D.Z., Wang, J.G., Qing, H.R., Yan, D.T., Li, R.W., 2009. Hydrothermal venting activities in the Early Cambrian, South China: petrological, geochronological and stable isotopic constraints. Chem. Geol. 258, 168–181. https://doi.org/10.1016/j.chemgeo.2008.10.016.

Chen, D.Z., Zhou, X.Q., Fu, Y., Wang, J.G., Yan, D.T., 2015. New U-Pb zircon ages of the Ediacaran-Cambrian boundary strata in South China. Terra Nova 27, 62–68. https://doi.org/10.1111/ter.12134.

Clark, S.H.B., Poole, F.G., Wang, Z., 2004. Comparison of some sediment-hosted, stratiform barite deposits in China, the United States and India. Ore Geol. Rev. 24, 85–101. https://doi.org/10.1016/j.oregeorev.2003.08.009.

Cooke, D.R., Bull, S.W., Large, R.R., McGoldrick, P.J., 2000. The importance of oxidized brines for the formation of Australian Proterozoic stratiform sediment-hosted Pb-Zn (Sedex) deposits. Econ. Geol. 95, 1–17. https://doi.org/10.2113/gsecongeo.95.1.1.

Emsbo, P., Johnson, C.A., 2004. Formation of modern and Paleozoic stratiform barite at cold methane seeps on continental margins: comment and reply: comment. Geology 32, e64–e65. https://doi.org/10.1130/0091-7613-32.1.e64.

Fakhraee, M., Hancisse, O., Canfield, D.E., Crowe, S.A., Katsev, S., 2019. Proterozoic seawater sulfate scarcity and the evolution of ocean–atmosphere chemistry. Nat. Geosci. 12, 375–380. https://doi.org/10.1038/s41561-019-0351-5.

Feng, Z.Z., Peng, Y.M., Jin, Z.K., Bao, Z.D., 2002. Lithofacies palaeogeography of the early Cambrian in China. J. Palaeogeogr. 4, 1–14 (in Chinese with English abstract).

Fernandes, N.A., Gleeson, S.A., Magnall, J.M., Creaser, R.A., Martel, E., Fischer, B.J., Sharp, R., 2017. The origin of late Devonian (Frasnian) stratiform and stratabound mudstone-hosted barite in the Selwyn basin, northwest territories, Canada. Mar. Pet. Geol. 85, 1–15. https://doi.org/10.1016/j.marpetgeo.2017.04.006.

Gigon, J., Deloule, E., Mercadier, J., Huston, D.L., Richard, A., Annesley, I.R., Wygralak, A.S., Skirrow, R.G., Mernagh, T.P., Masterman, K., 2020. Tracing metal sources for the giant McArthur River Zn–Pb deposit (Australia) using lead isotopes. Geology 48, 478–482. https://doi.org/10.1130/G47001.1.

Goodfellow, W.D., 1987. Anoxic stratified oceans as a source of sulphur in sediment-hosted stratiform Zn–Pb deposits (Selwyn basin, Yukon, Canada). Chem. Geol. 65, 359–382. https://doi.org/10.1016/0168-9622(87)90014-5.

Hanor, J.S., 2000. Barite–celestine geochemistry and environments of formation. Rev. Mineral. Geochem. 40, 193–275. https://doi.org/10.2138/rmg.2000.40.4.

Humphris, S.E., Klein, F., 2018. Progress in deciphering the controls on the geochemistry of fluids in seafloor hydrothermal systems. Annu. Rev. Mar. Sci. 10, 7.1–7.29. https://doi.org/10.1146/annurev-marine-121916-063233.

Jewell, P.W., Stallard, R.F., 1991. Geochemistry and paleoceanographic setting of Central Nevada bedded barites. J. Geol. 99, 151–170. https://doi.org/10.1086/629482.

Jewell, P.W., 2000. Bedded barite in the geologic record. In: Glenn, C.R., Prévôt-Lucas, L., Lucas, J. (Eds.), Marine Authigenesis: from Global to Microbial. In: SEPM Society for Sedimentary Geology, vol. 66, pp. 147–161.

Jin, C.S., Li, C., Algeo, T.J., Planavsky, N.J., Cui, H., Yang, X.L., Zhao, Y.L., Zhang, X.L., Xie, S.C., 2016. A highly redox-heterogeneous ocean in South China during the Early Cambrian (~529–514 Ma): implications for biota-environment co-evolution. Earth Planet. Sci. Lett. 441, 38–51. https://doi.org/10.1016/j.epsl.2016.02.019.

Johnson, C.A., Kelley, K.D., Leach, D.L., 2004. Sulfur and oxygen isotopes in barite deposits of the western Brooks Range, Alaska, and implications for the origin of the Red Dog massive sulfide deposits. Econ. Geol. 99, 1435–1448. https://doi.org/10.2113/gsecongeo.99.7.1435.

Johnson, C.A., Emsbo, P., Poole, F.G., Rye, R.O., 2009. Sulfur- and oxygen-isotopes in sediment-hosted stratiform barite deposits. Geochim. Cosmochim. Acta 73, 133–147. https://doi.org/10.1016/j.gca.2008.10.011.

Kampschulte, A., Strauss, H., 2004. The sulfur isotopic evolution of Phanerozoic seawater based on the analysis of structurally substituted sulfate in carbonates. Chem. Geol. 204, 255–286. https://doi.org/10.1016/j.chemgeo.2003.11.013.

Leach, D.L., Bradley, D.C., Huston, D., Pisarevsky, S.A., Taylor, R.D., Gardoll, S.J., 2010. Sediment-hosted lead-zinc deposits in Earth history. Econ. Geol. 105, 593–625. https://doi.org/10.2113/gsecongeo.105.3.593.

Li, C., Love, G.D., Lyons, T.W., Fike, D.A., Sessions, A.L., Chu, X., 2010. A stratified redox model for the Ediacaran ocean. Science 328, 80–83. https://doi.org/10.1126/science.1182369.

Li, D., Ling, H.F., Shields-Zhou, G.A., Chen, X., Cremonese, L., Och, L., Thirlwall, M., Manning, C., 2013. Carbon and strontium isotope evolution of seawater across the Ediacaran–Cambrian transition: evidence from the Xiaotan section, NE Yunnan, South China. Precambrian Res. 225, 128–147. https://doi.org/10.1016/j.precamres.2012.01.002.

Li, Z.X., Bogdanova, S.V., Collins, A.S., Davidson, A., Waele, B.D., Ernst, R.E., Fitzsimons, I.C.W., Fuck, R.A., Gladkochub, D.P., Jacobs, J., Karlstrom, K.E., Lu, S., Natapov, L.M., Pease, V., Pisarevsky, S.A., Thrane, K., Vernikovsky, V., 2008. Assembly, configuration, and break-up history of Rodinia: a synthesis. Precambrian Res. 160, 179–210. https://doi.org/10.1016/j.precamres.2007.04.021.

Lyons, T.M., Reinhard, C.T., Planavsky, N.J., 2014. The rise of oxygen in Earth's early ocean and atmosphere. Nature 506, 307–315. https://doi.org/10.1038/nature13068.

Magnall, J.M., Gleeson, S.A., Stern, R.A., Newton, R.J., Poulton, S.W., Paradis, S., 2016. Open system sulphate reduction in a diagenetic environment-isotopic analysis of barite (δ^{34}S and δ^{18}O) and pyrite (δ^{34}S) from the Tom and Jason late Devonian Zn–Pb–Ba deposits, Selwyn Basin, Canada. Geochim. Cosmochim. Acta 180, 146–163. https://doi.org/10.1016/j.gca.2016.02.015.

Maynard, J.B., Okita, P.M., 1991. Bedded barite deposits in the United States, Canada, Germany, and China: two major types based on tectonic setting. Econ. Geol. 86, 364–376. https://doi.org/10.2113/gsecongeo.86.2.364.

Ouyang, B., Renock, D., Akob, D.M., 2018. Effects of organic ligands and background electrolytes on barite dissolution. Geochim. Cosmochim. Acta 256, 6–19. https://doi.org/10.1016/j.gca.2018.02.003.

Paytan, A., Mearon, S., Cobb, K., Kastner, M., 2002. Origin of marine barite deposits: Sr and S isotope characterization. Geology 30, 747–750. https://doi.org/10.1130/0091-7613(2002)030<0747:OOMBDS>2.0.CO;2.

Poulton, S.W., Canfield, D.E., 2011. Ferruginous conditions: a dominant feature of the ocean through Earth's history. Elements 7, 107–112. https://doi.org/10.2113/gselements.7.2.107.

Sperling, E.A., Melchin, M.J., Fraser, T., Stockey, R.G., Farrell, U.C., Bhajan, L., Brunoir, T.N., Cole, D.B., Gill, B.C., Lenz, A., Loydell, D.K., Malinowski, J., Miller, A.J., Plaza-Torres, S., Bock, B., Rooney, A.D., Tecklenburg, S.A., Vogel, J.M., Planavsky, N.J., Strauss, J.V., 2021. A long-term record of early to mid-Paleozoic marine redox change. Sci. Adv. 7, eabf4382. https://doi.org/10.1126/sciadv.abf4382.

Torres, M.E., Bohrmann, G., Dubé, T.E., Poole, F.G., 2003. Formation of modern and Paleozoic stratiform barite at cold methane seeps on continental margins. Geology 31, 897–900. https://doi.org/10.1130/G19652.1.

Wang, J., Chen, D., Yan, D., Wei, H., Xiang, L., 2012. Evolution from an anoxic to oxic deep ocean during the Ediacaran–Cambrian transition and implications for bioradiation. Chem. Geol. 306–307, 129–138.

Wang, Z., Li, G., 1991. Barite and witherite deposits in Lower Cambrian shales of South China: stratigraphic distribution and geochemical characterization. Econ. Geol. 86, 354–363. https://doi.org/10.2113/gsecongeo.86.2.354.

Xu, L., Lehmann, B., Mao, J., Zhang, W., Ye, H., Li, H., 2016. Strontium, sulfur, carbon, and oxygen isotope geochemistry of the early Cambrian strata-bound barite and witherite deposits of the Qinling-Daba region, northern margin of the Yangtze Craton, China. Econ. Geol. 111, 695–718. https://doi.org/10.2113/econgeo.111.3.695.